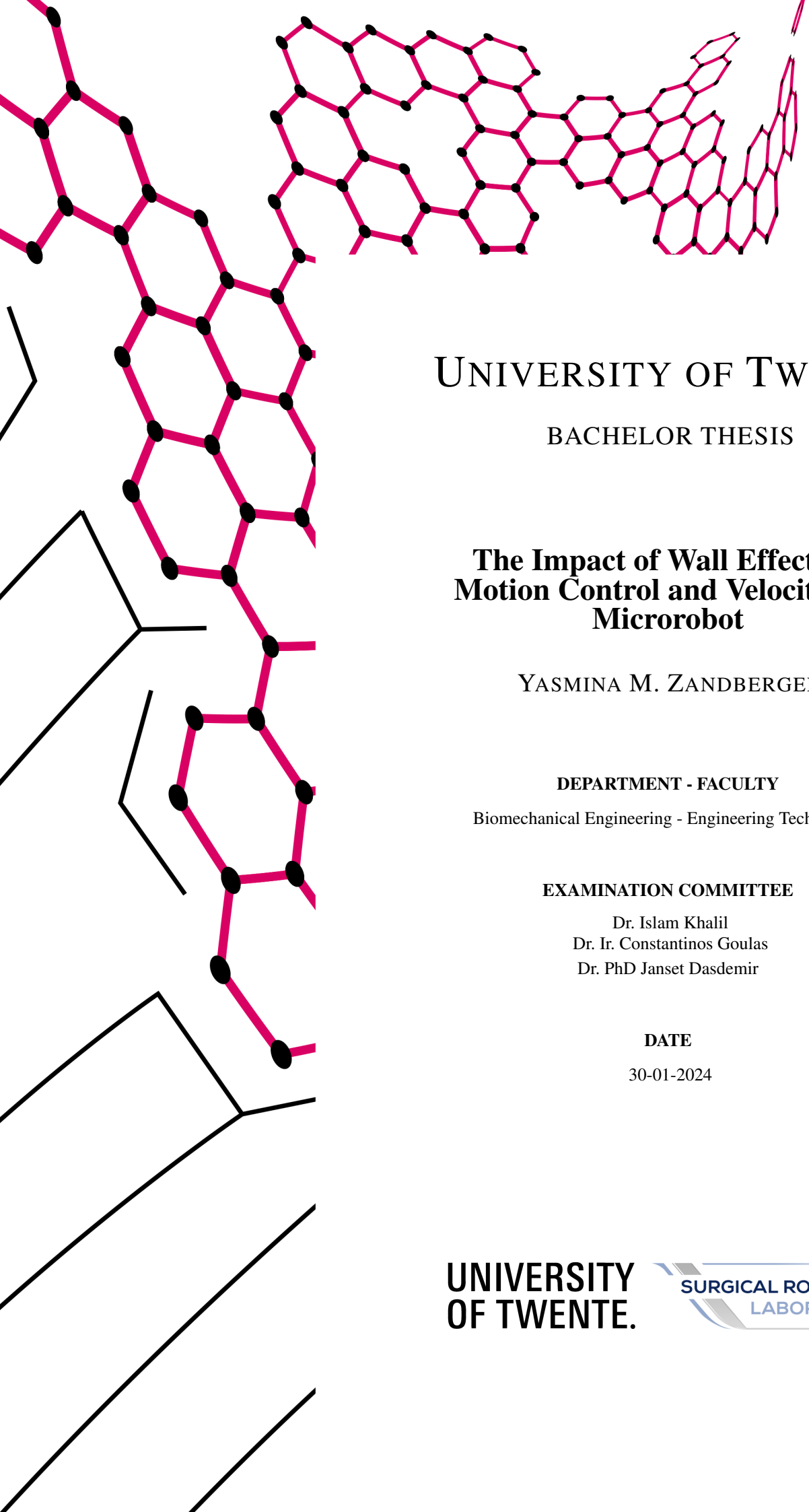

UNIVERSITY OF TWENTE

BACHELOR THESIS

The Impact of Wall Effects on Motion Control and Velocity of a Microrobot

YASMINA M. ZANDBERGEN

DEPARTMENT - FACULTY

Biomechanical Engineering - Engineering Technology

EXAMINATION COMMITTEE

Dr. Islam Khalil
Dr. Ir. Constantinos Goulas
Dr. PhD Janset Dasdemir

DATE

30-01-2024

UNIVERSITY OF TWENTE.

SURGICAL ROBOTICS LABORATORY

Contents

1 Abstract

Previous research on untethered helical magnetic devices (UHMDs) has focused on devices that are a millimeter in scale or larger. This study investigates the motion of a significantly smaller UHMD (microrobot) and examines the impact of wall effects on motion control and velocity in a low Reynolds number regime. Due to the microrobot's size, its motion is highly sensitive to factors such as magnetic field strength, rotation frequency, and positioning of the rotating permanent magnet in relation to the microrobot. The motion of the microrobot was investigated under three conditions: in bulk fluid, confined by one surface, and confined by two surfaces. The experimental results indicate that motion control is optimized when the microrobot is confined by two surfaces. However, discrepancies arise when predicting increased velocity with increasing actuation frequency and reduced confinement. The results demonstrate that forward velocity is not influenced by the given condition. Theoretical models were used to confirm the expected velocities, which do confirm the relationship between the condition and velocity, but show a deviation by a factor of approximately 10. The results of this study are significant for the use of microrobots in minimally invasive procedures that require precise motion control.

2 Introduction

Medical procedures can be improved by modifying them to be less invasive or by developing new procedures. A less invasive procedure can assist the patient by reducing recovery time, the number of complications, the risk of infection, and postoperative pain [1] [2] [3]. This study investigates a specific type of untethered helical magnetic devices (UHMD). UHMDs are magnetically activated helical microrobots, also known as microrobots. It is intended that these microrobots will enable minimally invasive procedures in hard-to-reach locations [1] [2] because of their ability to travel through fluid-filled lumens and cavities as well as soft tissue to the target site [1]. The use of a microrobot allows for the improvement of procedures such as targeted drug delivery or tissue removal [2] [4].

The design of microrobots is based on microorganisms that move through fluids by rotating their helical flagella, such as Escherichia coli [5], bacteria, microalgae, and spermatozoa [2] [5]. The propulsion mechanism used by these microorganisms allows them to move through a fluid at a low Renolds number ($\mathrm{Re} \equiv \mathrm{UL}\rho/\mu < 1$). Where U is the velocity, L is the characteristic length, ρ is the density and μ is the kinematic viscosity of the fluid [4]. In this study, the microrobot consists of a helix-shaped tail and a hemispherical head. Figure 2 shows a SEM image of the microrobot used [6]. The design of the head can be customized for a specific task, such as pushing or pulling a specific application. The design can also be chemically treated for drug delivery [4].

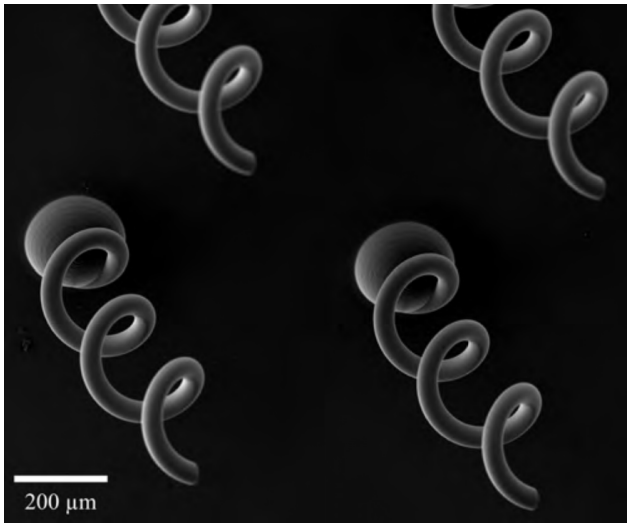

Figure 2: The microrobot visualised with a SEM microscope [6].

The microrobot propels itself by rotating around its helical axis, which is induced by an external rotating magnetic field generated by a rotating permanent magnet (RPM). The RPM's positioned in a way that the rotation axis is parallel to the microrobot's rotation axis, as shown in Figure 3(a). The orientation of the magnetic field relative to the microrobot is shown in Figure 3(b).

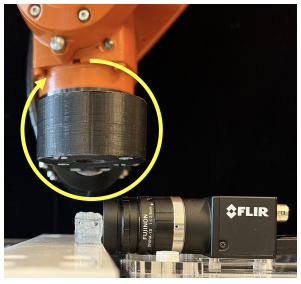

(a) The microrobot is actuated by a single RPM fixed to a robotic arm. The RPM is positioned precisely above the container holding the microrobot. The yellow arrow indicates the RPM's rotation.

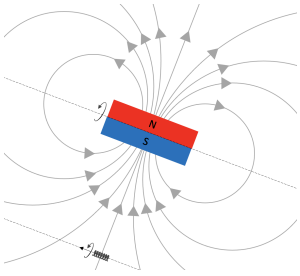

(b) The microrobot moves through the magnetic field perpendicular to the field lines. Rotation of the RPM around the rotation axis causes the microrobot to rotate around its helical axis.

Figure 3: The relationship between RPM and microrobot.

A microrobot is able to move through fluid-filled lumens and cavities, and soft tissue [1]. The focus of this study is on the movement of the microrobot in fluid-filled lumens. Several forces (a drag force, a magnetic force and a force due to gravity) act on the microrobot during its movement. These forces are in balance [7]. As the microrobot moves from the insertion point to the target site, the lumen wall constrains the movement. During this movement, the distance to the wall may vary. The drag force varies with the distance from the confining wall [8]. This is known as the wall effect. Understanding the impact of wall effects is crucial for gaining control over the motion of the microrobot since these wall effects affect the force balance and, consequently, the motion and velocity of the microrobot. This impact is investigated for a microrobot of 1.17 mm to answer the research question: "What is the impact of wall effects on the velocity and the motion control of a microrobot? The question is answered by studying how the microrobot responds to moving under three different conditions. (1) The motion in the bulk of the fluid, (2) the motion when the microrobot is confined by one surface, (3) and the motion when the microrobot is confined by two perpendicular surfaces.

Knowledge of larger UHMDs is used to predict and theoretically model the response of this microrobot under various conditions. These UHMDs move forward in the same way as the microrobot used, i.e. along the helical axis due to a rotation around their helical axis [4]. Based on this knowledge, it is hypothesized that the third condition is optimal for motion control because the motion is limited to a specific trajectory. Additionally, it is expected that the first condition will result in the highest velocity due to the lower drag force. Finally, it is expected that the velocity will increase with an increasing actuation frequency of the RPM.

To theoretically support the results of the experiments, the response of the microrobot to the different conditions is modeled using Matlab. This model is based on the model of Gray and Hancock (1955) and Lighthill (1976). Gray and Hancock and Lighthill developed a resistive force theory (RFT) to describe helical swimming at low Renolds number. This theory is already used to interpret propulsion by a planar wave in sperm, small worms, Chlamydomonas reinhardtii, and swimmers in a granular material [9]. This RFT model is adapted to the characteristics of the microrobot and to the three conditions. An evaluation of the experimental and modeled results provides a comprehensive analysis of the impact of wall effects on motion control and velocity.

3 Theory

A model developed by L.W. Ligtenberg based on the RFT developed by Gray and Hancock is used to predict the velocity of the microrobot [7] [10]. The model demonstrates a force and torque balance that applies to a microrobot swimming at a low Reynolds number in an open fluidic environment [7]. The model is adapted to the three conditions: motion in the bulk of the fluid, motion confined by one surface, or motion confined by two surfaces. The model and its adaptations are described in this chapter.

3.1 Force and Torque Balance

The motion of the microrobot is influenced by three forces: gravity ($\mathbf{F}_g$), drag force ($\mathbf{F}_d$), and magnetic force ($\mathbf{F}_m$). Gravity affects the microrobot due to its higher density compared to water. Drag force is the resistance to motion caused by the fluidic environment. The magnetic force enables the movement. These forces produce corresponding torques ($\boldsymbol{\tau}_g$, $\boldsymbol{\tau}_d$ and $\boldsymbol{\tau}_m$, respectively). Both the torques and the forces are balanced, this is described as follows [7]:

$$\begin{pmatrix} \mathbf{F}_m + \mathbf{F}_d + \mathbf{F}_g \\ \boldsymbol{\tau}_m + \boldsymbol{\tau}_d + \boldsymbol{\tau}_g \end{pmatrix} = \mathbf{0} \tag{1}$$

Incorporating the wall effects into the model alters the drag force $\mathbf{F}_d$ to $\mathbf{F}_{d,1S}$ or $\mathbf{F}_{d,2S}$ for the movement confined by one, or two surfaces, respectively. Incorporating the wall effects alters the drag torque $\boldsymbol{\tau}_d$ to $\boldsymbol{\tau}_{d,1S}$ or $\boldsymbol{\tau}_{d,2S}$ as well for the movement confined by one, or two surfaces, respectively.

The forces have an orientation. The drag force is in the opposite direction of movement. The direction of the magnetic force aligns with the direction of the microrobot's position vector relative to the RPM ($^a\mathbf{p}_h$). The force of gravity acts in the direction of the negative z-axis. The orientations are visualised with the red arrows in Figure 4. The torques have an orientation perpendicular to the orientation of the forces.

3.2 Gravitational Force and Torque

The inspiration for the microrobot is taken from cellular micro-swimmers. These micro-swimmers consist generally of a fluid with the density close to water. This is not the case for the microrobot which consists

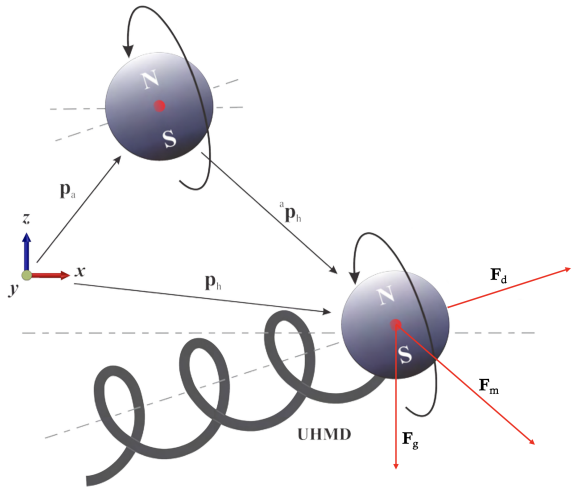

Figure 4: The forces acting on the microrobot and the orientation of the forces characterized with respect to a frame of reference x,y,z.

of materials denser than water [4]. This means that the weight is non-neglectible and that there is a need to compensate for gravity [11]. The force due to gravity in a fluid can be expressed as follows:

$$\mathbf{F}_g = (\rho_r - \rho_f) * g * V; \tag{2}$$

Here, ρ_r denotes the density of the microrobot and ρ_f denotes the density of the fluid. V denotes the volume and g the gravitational acceleration.

3.3 Drag Force and Torque

The motion of the microrobot is affected by its environment, in this case the fluid or the fluid near surface(s) it is in. The fluid gives a resistance to the motion, this is known as drag [12].

3.3.1 Bulk

The drag force during the motion in the bulk of the fluid is obtained by integrating Equation 3 over an infinitely small element of the helix (ds). ϕ denotes the orientation of this infinitely small element [12]. This results in the following the drag force (Eq. 4):

$$dF_d = C_T\, \mathbf{v}_h \sin\phi\, ds \tag{3}$$

$$\mathbf{F}_d = C_T L\, \mathbf{v}_h \cos\theta \tag{4}$$

In which $\mathbf{v}_h$ denotes the axial velocity, C_T the drag coefficient, L the body length and θ the pitch angle of the helix. The drag coefficient can be be expressed as:

$$C_T = \frac{2\pi\mu}{ln\frac{2\lambda}{a} - \frac{1}{2}} \tag{5}$$

Where μ is the viscosity of the fluid, λ the pitch of the helix and a the radius of the helical wire. Converting the drag force to its corresponding torque gives the following equation:

$$\boldsymbol{\tau}_d = (\omega_h R^2)(C_T \sin^2\theta)\frac{L}{\cos\theta} \tag{6}$$

Here, R is the radius of the coil.

3.3.2 Confined by one Surface

The closer the microrobot is to a surface, the greater the drag force the microrobot will experience. This means that as the microrobot is rotating near a surface, the forces on a infinitely small element changes over time due to a changing distance to the surface. These different forces on different parts of the microrobot cause a drag anisotropy [8] [13]. The anisotropy results in a lateral drift [4]. To model this anisotropy, the drag coefficents are altered based on a force analysis. The force analysis focuses on the surface parallel to the helical axis and simplifies the microrobot to a cilindrical slender rod (radius R). The drag coefficients are based on the RFT and slender body modeling (SBM), and described as follows [8] [14]:

$$C_X = \frac{4\pi\mu}{ln\frac{2h}{R}} \tag{7}$$

$$C_Y = \frac{2\pi\mu}{ln\frac{2h}{R}} \tag{8}$$

$$C_Z = \frac{4\pi\mu}{ln\frac{2h}{R} - 1} \tag{9}$$

The drag coefficients are calculated based on the distance between the microrobot and the surface (h) rather than the pitch of the helix. It is important to note that the distance h is much smaller than the body length (L). The subscripts (X, Y and Z) denote the direction. The lateral drift is mainly influenced by C_Z, which is the drag coefficient in the direction perpendicular to the surface [8]. To determine the drag force when the motion of the microrobot is confined by one surface, C_T in formula 3 is replaced by C_Z and integrated over ds which gives rise to the following Equation:

$$\mathbf{F}_{d,1S} = C_Z L\, \mathbf{v}_h \cos\theta \tag{10}$$

This is again translated to torque, which gives rise to the following:

$$\boldsymbol{\tau}_{d,1S} = (\omega_h R^2)(C_Z \sin^2\theta)\frac{L}{\cos\theta} \tag{11}$$

Both the drag force and the torque are now dependent on the distance to the surface (h).

3.3.3 Confined by two surfaces

If the motion of the microrobot is confined by two perpendicular surfaces, it is assumed that the drag forces due to a single surface can be added together. Thus, for a motion in x-direction, with surfaces in the z- and y-plane, C_Z and C_Y determine the drag force. This results in the following:

$$\mathbf{F}_{d,2S} = \mathbf{v}_h \, L(C_Z \cos\theta + C_Y \cos\theta) \tag{12}$$

This gives the following corresponding torque:

$$\boldsymbol{\tau}_{d,2S} = (\omega_h R^2)(C_Z \sin^2\theta + C_Y \sin^2\theta)\frac{L}{\cos\theta} \tag{13}$$

The drag force and torque again depend on the distance to the surface, but the drag force will be greater.

3.4 Magnetic Force and Torque

The RPM applies a rotating magnetic field. The amount of magnetic force that the microrobot experiences is dependent on its position within the magnetic field (${}^a\mathbf{p}_h$). The closer to the RPM, the greater the magnetic force. The equations for magnetic force ($\mathbf{F}_m$) and the magnetic torque ($\boldsymbol{\tau}_m$) are stated below:

$$\mathbf{F}_m = (\mathbf{m}_h \cdot \nabla)\mathbf{B}({}^a\mathbf{p}_h) \tag{14}$$

$$\boldsymbol{\tau}_m = \mathbf{m}_h \times \mathbf{B}({}^a\mathbf{p}_h) \tag{15}$$

The magnetic force and torque depend on the dipole moment ($\mathbf{m}_h$) and magnetic flux density ($\mathbf{B}$). To construct the magnetic flux density, the following equation is used:

$$\mathbf{B}({}^a\mathbf{p}_h) = \frac{\mu_0}{4\pi \mathbf{p}_h^5}(3\mathbf{p}_h\mathbf{p}_h^T - \mathbf{p}_h^2\mathbf{I})VM \tag{16}$$

Where μ_0 is the permeability of free space, and $\mathbf{I}$ is an identity matrix. The position ${}^a\mathbf{p}_h$ is expressed as position vector:

$${}^a\mathbf{p}_h = [{}^a\mathbf{p}_{h_x}, {}^a\mathbf{p}_{h_y}, {}^a\mathbf{p}_{h_z}]^T \tag{17}$$

The orientation of the microrobot to the RPM are also visualised in figures 4 and 5

3.5 Velocity

To obtain the axial velocity ($\mathbf{v}_h$) the balance needs to be solved for the drag force, as the axial velocity is a component of the drag force. The orientation of $\mathbf{v}_h$ is visualised in figure 5.

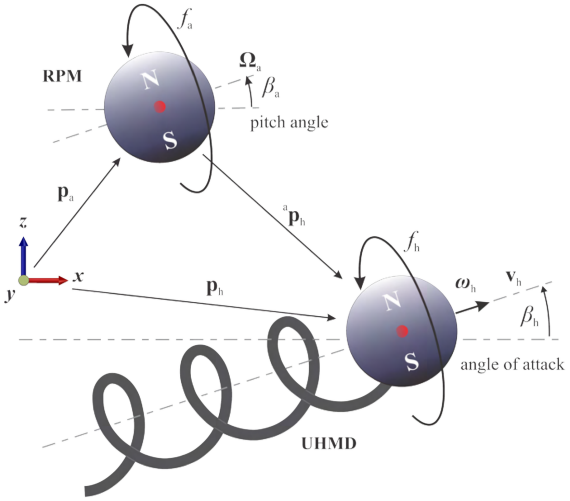

Figure 5: The velocities $\mathbf{v}_h$ is in line with the rotation axis ω_h of the microrobot. Both characterized with respect to a frame of reference x,y,z [15]

3.6 Step-out Frequency

When the magnetic torque and opposing drag torque are exactly equal to eachother ($\boldsymbol{\tau}_m = \boldsymbol{\tau}_d$), the microrobot exhibits a step-out frequency. This frequency marks a crucial turning point of the swimming behavior of the microrobot. Below this rotational frequency of the magnetic field (f_a), the magnetic torque is greater than the drag torque. This means that the magnetic torque is able to counterbalance the drag torque, resulting in the rotational frequency of the RPM being equal to the rotational frequency of the microrobot (f_b)(Fig. 5). Above the step-out frequency, the magnetic torque is not able to counterbalance the drag torque, resulting in an asynchronous rotation frequency. To obtain the step-out frequency, ω_h in the equation for $\boldsymbol{\tau}_d$ is rewritten to $2\pi f_0$. Where f_0 denotes the step-out frequency [12].

4 Method

To investigate the impact of wall effects on motion control and velocity, experiments were conducted to obtain frequency responses for the three conditions. This chapter discusses the methods used in these experiments.

4.1 Experimental Method

4.1.1 General Setup

The microrobot is placed in a rectangular container filled with water. The method for obtaining the frequency response varies depending on the condition. To

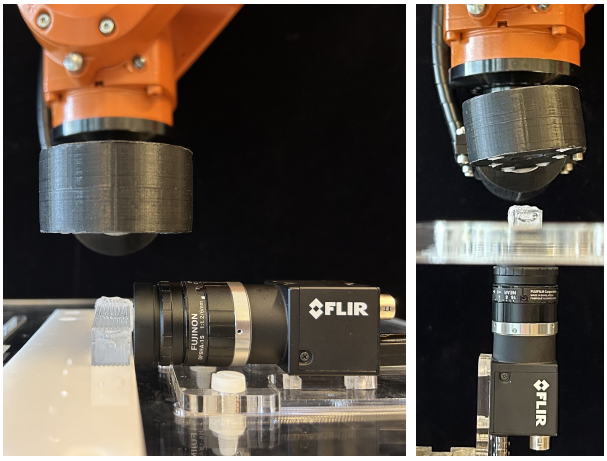

(a) Bulk & Confined by two surfaces

(b) Confined by one surface

Figure 6: Experimental setup for the different conditions, showing the RPM, the Flir camera, and the container with the microrobot.

investigate motion in the bulk of the fluid, a launch pad is created in the container. This launch pad was not necessary for the other conditions. Figure 6 displays the experimental setup for each condition.

4.1.2 Frequency Response in Bulk

The microbot's movement in bulk begins from its starting position on the launchpad, which is manually set. The distance from the starting position to the RPM (z) is determined through trial and error. The objective was to determine the distance z at which the microrobot travels at a constant distance from the launch pad to the end position ($\pm$ 20 seconds later). This resulted in an initial distance of 4.87 cm. Maintaining the distance of 4.87 cm was not possible as it resulted in upward and downward movements, as shown in trajectories B_a and B_b in Figure 7, but the distance of 4.87 cm allowed both events to occur as late as possible. This means that the microrobot would move at this distance for the maximum possible duration. Starting from 20Hz, it was observed that the microrobot only moved downwards. As a result, the value of z was reduced to 4.80. At this distance, the microrobot consistently moves upwards until 15 Hz, after which it moves randomly both upwards and downwards.

To obtain the frequency response, the velocity of the movement was measured while increasing the actuation frequency of the RPM from 5 to 35 Hz with 5 Hz intervals. The RPM remained stationary during the experiment. The movement of the microrobot was documented using a FlirCamera and these video's were analysed using the Tracker application. Tracker measured the microrobot's position in the video frames and used a reference distance to measure the amount of change in position in all frames. The velocity was acquired using Matlab.

4.1.3 Frequency Response Confined by One Surface

To analyze the movement of the microrobot when it is confined by one surface, its movement over the bottom surface is documented. Therefore, the FlirCamera is positioned in line with the container and RPM as shown in Figure 6(b). The bottom surface was chosen instead of the top surface to minimize the "pulling" effect of the RPM. However, dust and other inconsistencies on the surface would randomly hinder the movement of the microrobot. An attempt was made to achieve a circular trajectory for the microrobot, taking into account its tendency to drift until it is confined by two surfaces where it moves forward or backward. The circular trajectory, as shown in Figure 7(b), was achieved by rotating the RPM clockwise for 25 seconds. At 25 seconds, the RPM rotation direction was changed to counterclockwise rotation for 25 seconds.

For this experiment, the initial distance (z) between the RPM and the microrobot is 4.90 cm. To obtain the velocity, the method explained in section 4.1.2 was applied. The actuation frequency was increased from 5 to 30 Hz in 5 Hz intervals.

4.1.4 Frequency Response Confined by Two Surfaces

To analyze the movement of the microrobot when it is confined by two surfaces, again a frequency response is conducted. Therefore, the RPM is positioned at two different distances from the microrobot. At a starting distance of 5.05 cm, the motion is confined by the bottom - and side surface. At a starting distance of 4.15 cm, the motion is confined by the top - and side surface. The motion along the two surfaces was recorded for 20 seconds after the motion was initiated. The trajectory of the microrobot is depicted in figure 7(c).

For both distances, the velocity was obtained by applying the method explained in section 4.1.2. However, this time the actuation frequency is increased from 5 to 32 Hz with 1 Hz intervals.

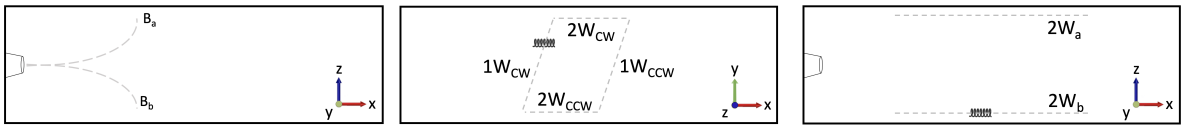

(a) Bulk *(b) Confined by one surface* *(c) Confined by two surfaces*

Figure 7: The trajectories are depicted with the gray line. (a) and (c) are in the x,z-plane. The denominator a denotes the upside of the container, b denotes the downside of the container. (b) is in the x,y-plane. The denominator CW denotes a clockwise rotation of the RPM and CCW a counterclockwise rotation of the RPM.

4.2 Method for the Theoretical Model: Matlab Model

A theoretical model is used to calculate the theoretical velocities using an expected trajectory. The model is based on the formulas described in chapter 3.

4.2.1 Motion Control

Motion control refers to the ability to manage motion by controlling inputs. In these experiments, motion control is measured by the degree to which the microrobot's trajectory deviates from the expected trajectory. The expected trajectories differ for each condition. For motion in the bulk of the fluid, it is expected that the distance between the microrobot and the RPM remains constant in the z-direction. The microrobot remains directly beneath the RPM, resulting in a constant y-direction distance of 0. However, the x-direction distance does vary (around 3 body lengths). In the case of motion confined by one surface, the coordinates change in all directions during movement. In the case of motion confined by two surfaces, the distance in the z-direction changes, as well as the distance in the x-direction (around 3 body lengths). The y-direction distance remains constant at 0. Motion control is tested by observing the trajectories.

4.2.2 Average Velocity per Condition

To model the average velocity, the force balance described in equation 1 is used to calculate the drag force. In this balance, F_g is a constant and F_m is varying with distance to the RPM. The positions used to calculate the magnetic force are on the expected trajectory, which is described in section 4.2.1. After calculating the drag force, the velocity components are taken out of the drag force equations (4, 10 and 12) to calculate those. The velocity is then calculated for a series of positions along the expected trajectory. To calculate the average velocity, the mean of these velocities is taken.

5 Results

The experiments of three conditions resulted in frequency responses of the microrobot to the actuation frequency. These results and the derived results of these frequency responses are discussed in the experimental results. The theoretical model resulted in average velocities per condition, which are discussed in the theoretical results.

5.1 Experimental Results

The motion in bulk and the motion confined by one surface can be divided in a movement in x-direction and a movement in y- or z-direction. This means that total velocity can be divided into velocities in those directions as well. The motion confined by two surfaces can not be divided into velocities in two different directions, since it is confined to only a movement with a velocity in x-direction. The velocity in the x-direction represents the speed at which the microrobot will move from the insertion point. the target site in a vessel.

The frequency responses in the three conditions are visualised in figure 8. In this figure, (a) and (b) are the results of the movement in Bulk, (c) and (d) are the results of the movement confined by one surface and (e) is the result of the movement confined by two surfaces.

5.1.1 Frequency Response in Bulk

The frequency response of the movement in the bulk of the fluid shows that the average total velocity is more influenced by the average velocity in the z-direction than in the x-direction. This effect is particularly evident in the frequency response, where the microrobot ultimately moves in the direction of the RPM, with the starting distance of 4.80 cm. In the results of this experiment, the average velocity in z-direction and the average total velocity do substantially decrease with an increasing actuation frequency (63,7%). In the measurement with a starting distance of 4.87 cm, the average velocity and the total average velocity are

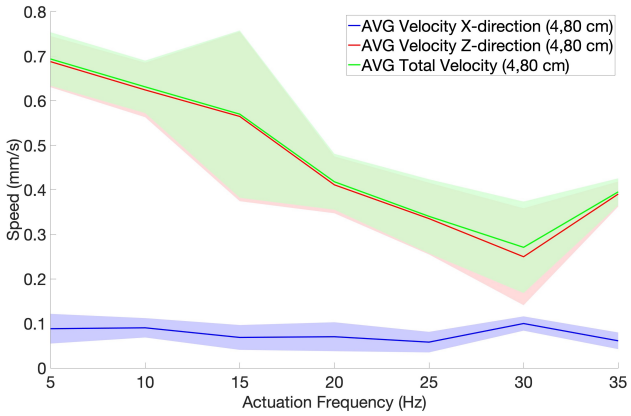

(a) The frequency response of the microrobot in bulk when it moves in the direction of the RPM.

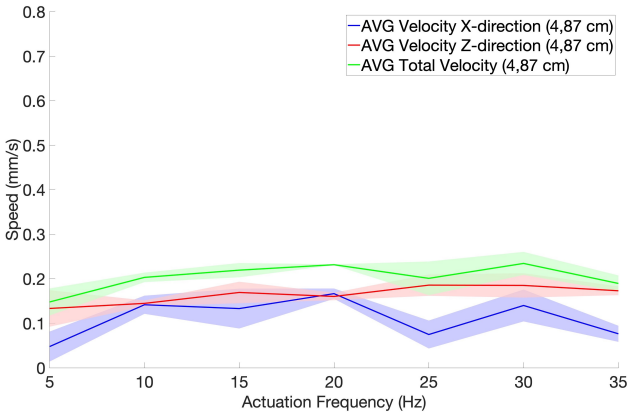

(b) The frequency response of the microrobot in bulk when the movement is dominated by gravity.

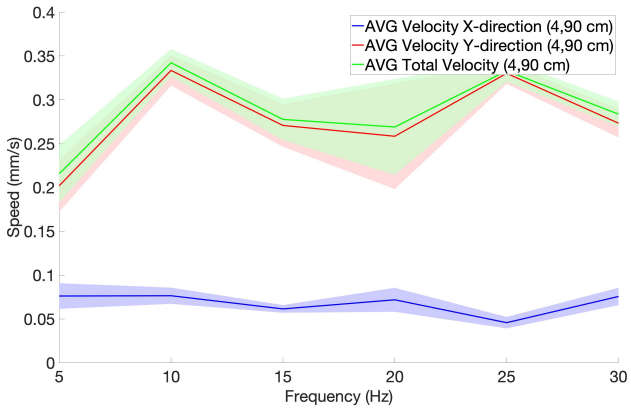

(c) The frequency response of the microrobot confined by one surface with the clockwise rotation frequency of the RPM.

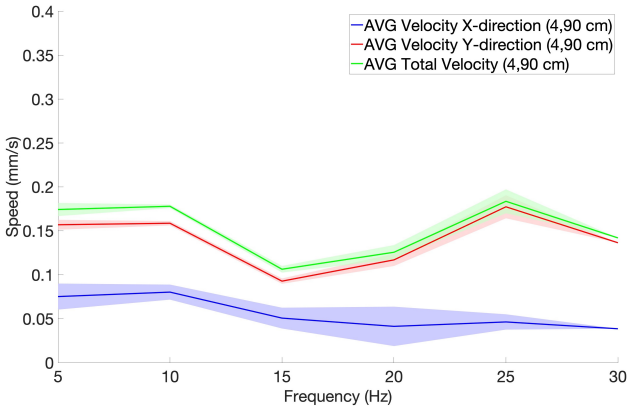

(d) The frequency response of the microrobot confined by one surface with the counterclockwise rotation frequency of the RPM.

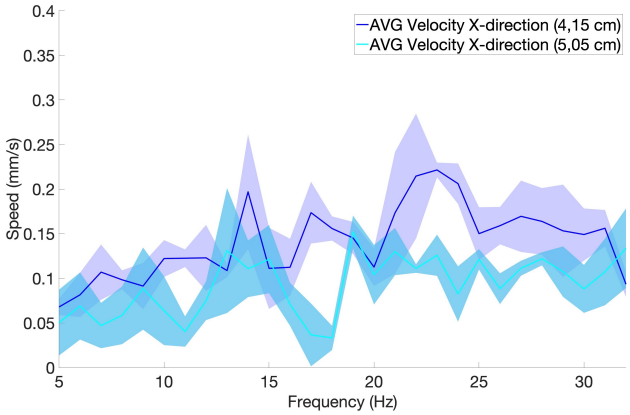

(e) The frequency response of the microrobot constricted by two surfaces, with two different distances to the RPM

Figure 8: The frequency responses of the microrobot to the actuation frequency in the three different conditions. The area represents the standard deviation of the mean. The line represents the mean.

constant over the actuation frequencies. The average velocity in x-direction is constant around 0.1 mm/s for both distances to the RPM.

5.1.2 Frequency Response Confined by One Surface

The frequency response of the movement constricted by one surface is executed at a starting distance of 4.90 cm to the RPM. In this case, a distinction was made between the clockwise and counterclockwise velocity.

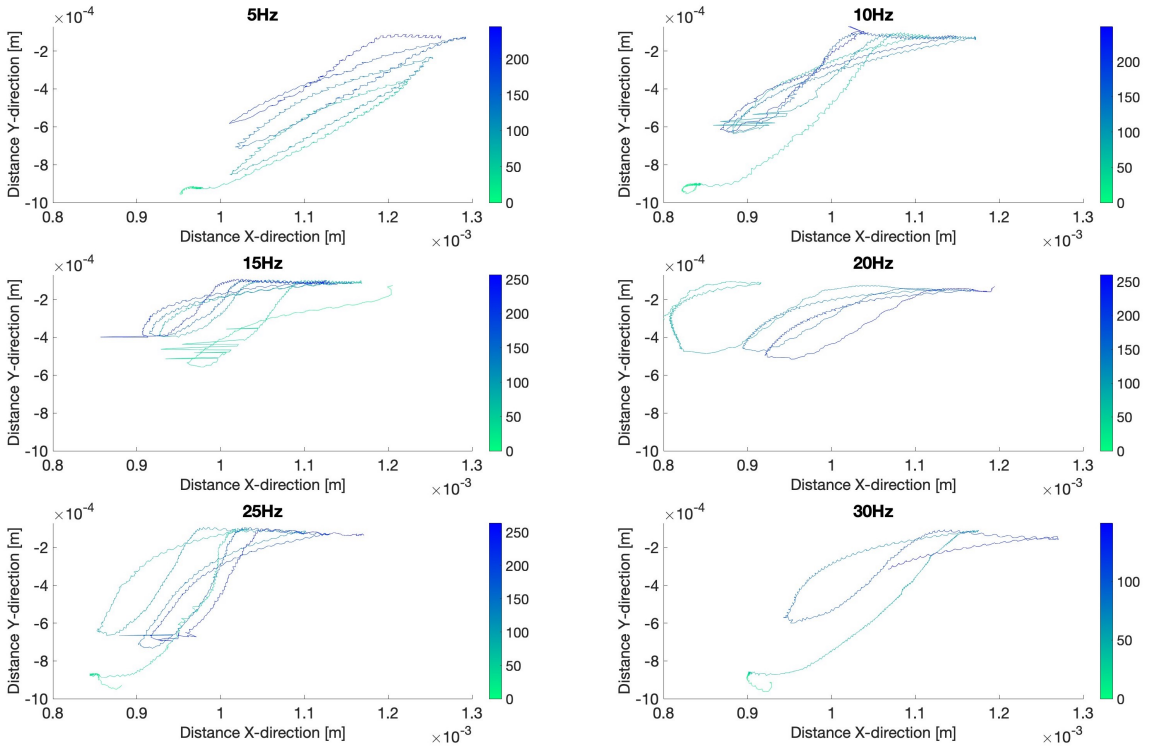

Figure 9: The trajectory of the microrobot during the lateral drift experiment. Plotted separately for all the frequencies, varying from 5 - 30 Hz. The time corresponding to each position is represented in the colorbar to the right of the graph.

The measurement at 30 Hz was not totally completed due to the maximum of the rotation frequency of the RPM. This means that there is only one valid value for the counterclockwise movement, note the standard deviation of 0. There were three valid repetitions for the clockwise movement, but done in 2 separate measurements instead of one.

In figures 8(c) and (d) it can be seen that the clockwise movement has a higher average velocity in y-direction and average total velocity than the counterclockwise movement. Both rotation directions do not show a specific relation between the average velocities and the actuation frequency. The average velocity in x-direction is constant around 0.06 mm/s in both rotation directions.

The trajectory of the microrobot during these measurements is plotted in figure 9. The time duration of the movement is shown in the colorbar next to the graphs. As shown in the figure, repeating the movement of changing the rotation direction gives similar trajectories. The microrobot's trajectory does not fully correspond to the expected movement, as it does not move completely from one side of the container to the other.

5.1.3 Frequency Response Confined by Two Surfaces

The frequency response of the movement confined by two surfaces results in an average velocity in the x-direction. Figure 8(e) shows that the average velocity with distance 4.15 cm between the microrobot and the RPM, is higher than the average velocity with distance 5,05 cm for almost all frequencies. There is in both measurements a small increase in average velocity in the first 10-15 Hz, but averages to 1.6 mm/s (4,.5 cm) and 1.0 mm/s (5.05 cm).

5.1.4 Frequency Response of the Three Conditions

Comparing the three conditions, the results show a similar average velocity in x-direction for all three conditions, in both behaviour and amount. The average total velocities differ substantially, with the highest average total velocity observed in bulk (4,80 cm) and the lowest average total velocity observed in the counterclockwise rotation frequency (4,90 cm). The average velocity in z-direction and the average total velocity in bulk (4,80 cm) is the only measurement which shows a relation between the average velocity and the actuation frequency. The other measurements did not show a relation, they stayed quite constant.

Table 1: Average velocity per condition

Condition	Experimental $\mathbf{v}_h$	Theoretical $\mathbf{v}_h$
Bulk (4.80)	0.488 mm/s	8.449 mm/s
Bulk (4.87)	0.206 mm/s	8.447 mm/s
1S CW (4.90)	0.287 mm/s	1.732 mm/s
1S CCW (4.90)	0.152 mm/s	1.732 mm/s
2S (4.15)	0.119 mm/s	1.380 mm/s
2S (5.05)	0.0916 mm/s	1.372 mm/s

5.2 Theoretical Results

5.2.1 Motion Control

For motion control, the experimental trajectories are compared to the expected and used theoretical trajectories. When observing the movement during the experiments, the movement confined by two surfaces is moving in a straight line alongside the two surfaces. The microrobot moves diagonally when confined by one surface, but it does not reach both sides of the container. For the bulk motion, the distance between the RPM and the microrobot decreases when starting at a distance of 4.80 cm and increases when starting at a distance of 4.87 cm.

5.2.2 Average Velocity

The theoretical model calculated the average velocity during the movement as well. The results are presented in table 1. The average velocities of the theoretical model are significantly higher (by a factor of around 10) than those of the experiments. The condition with the highest experimental velocity matches the condition with the highest theoretical velocity. This relation also applies to the other conditions. The variations within a condition show greater differences in the experimental results than in the theoretical results. However, even in these variations, the relationship remains consistent. The only exception to this rule is the clockwise and counterclockwise rotation when the motion is confined by one surface. The direction of rotation does not affect the theoretical average velocity.

6 Discussions

This study provides insight into the dynamics of a microrobot. The microrobot used in this case is much smaller than those used in other studies. However, the hypotheses are developed are based on the outcomes of these studies. The discussion includes experimental outcomes, the assumptions and considerations for practical applications, with a particular emphasis on motion control and velocity of the microrobot.

6.1 Motion control and Velocity

The results show that the motion of the microrobot confined by two surfaces is moving as expected. The motion confined by one wall is moving as expected when it is indeed confined by one wall, but because it does not reach the both sides of the container, it deviates a bit. For the motion in bulk, it was expected that the distance between the microrobot and the RPM will stay the same for the entire movement. This is not the case. These results supported the hypothesis that motion is more controlled when confined by two surfaces. However, the experimental results did not support the hypotheses that predicted an increase in velocity in the x-direction with increasing actuation frequency and reduced confinement due to lower drag forces. The observed velocities did not exhibit the anticipated correlation with frequency or confinement levels. One possible reason for this inconsistency is the decrease in magnetic field strength as the actuation frequency increases. The inconsistency in the increase of velocity in the x-direction may be due to the trust forward being too small compared to the pulling force of the RPM or the influence of gravity. That is, if the velocity in x-direction is assigned to the thrust forward and the velocity in y-direction is assigned to the pulling force of the RPM or the influence of gravity on the microrobot.

The theoretical average velocities exhibit a deviation from the experimental average velocities by a factor of approximately 10. This difference may be due to inaccuracies in model assumptions, experimental procedures, or scaling factors.

6.2 Assumptions

The study assumes that the drag force affecting the motion of the microrobot confined by two surfaces simply adds up. However, this claim is not supported by any source. The experimental results are used to test the validity of this theoretical assumption, and the relation between the amount of confinements looks similar, but this does not necessarily mean that the assumption is correct.

The study assumes that if the motion of the microrobot is confined by a flat surface, it produces the same results as motion confined by a curved surface due to the small size of the microrobot. The container used

allowed for videotaping with less distortion than videotaping the movement in a curved tube.

6.3 Considerations for Practical Applications

The study presents significant implications for practical applications. The experiments demonstrated that dust particles and other inconsistencies in the fluid have a significant impact on the motion of microrobots. The microrobot may become stuck temporarily or indefinitely due to the impact of this inconsistency. At present, it is not possible to visualize the microrobot as it is used in a practical application. If the microrobot were to move out of the reach of the applied magnetic field unintentionally (due to an inconsistency), retrieval would be difficult.

In all conditions, slight deviations in one of the inputs, such as field strength, actuation frequency, and positioning of the RPM with respect to the microrobot, can result in different outcomes. This shows how sensitive the microrobot is. Previous studies suggest that achieving bounded output is possible, but even small deviations can cause undesirable outcomes. Due to the small size of this microrobot, these deviations become even more critical, making it almost impossible to achieve the perfect combination of inputs. Undesirable outcomes, such as attraction towards the RPM or falling due to gravity, will almost always occur. When confined by one or two surfaces, the microrobot's ability to deviate from the expected trajectory is reduced, resulting in lower sensitivity. However, even with confinement to one surface, a difference in clockwise and counterclockwise velocity was observed. This difference may be related to the microrobot's starting position in relation to the RPM or the orientation (forward or backward) of the microrobot's movement.

7 Conclusions

The motion of a microrobot actuated by a single RPM is affected by wall effects. This phenomenon was studied under three different conditions. The experimental results indicate that motion control is optimal when the motion is confined by two surfaces. No preference can be stated for a specific condition regarding the velocity in the forward direction. The total velocity is highest when moving in the bulk of the fluid.

Previous studies suggest that achieving bounded output in bulk is possible, but even slight deviations from the optimal combination of inputs (such as field strength, actuation frequency, and positioning of the RPM with respect to the microrobot) can result in poor outcomes. Due to the small size of this microrobot, these deviations become even more critical, making it almost impossible to achieve the perfect combination of inputs. Undesirable outcomes such as attraction towards the RPM or falling due to gravity will almost always occur. Additionally, dust and other inconsistencies in the fluid can cause complications. Therefore, motion of this microrobot in the bulk of the fluid is not recommended. Further investigation into obtaining a bounded output and into the reaction of the motion of the microrobot to other fluids is necessary.

Confinement seemed promising due to the microrobot's sensitivity to motion in bulk. Positive forward velocity in all conditions suggests predictable motion is possible in fluid-filled vessels, provided they lack branching or wall inconsistencies. Confinement by two surfaces appears most promising. Promising results may be obtained by further investigation of tighter confinement and reducing the distance between the RPM and the microrobot.

References

[1] Nelson BJ, Kaliakatsos IK, Abbott JJ. Microrobots for minimally invasive medicine [Journal Article]. Annu Rev Biomed Eng. 2010;12:55-85. Available from: https://www.ncbi.nlm.nih.gov/pubmed/20415589. doi:10.1146/annurev-bioeng-010510-103409.

[2] Singh AV, Ansari MHD, Mahajan M, Srivastava S, Kashyap S, Dwivedi P, et al. Sperm Cell Driven Microrobots-Emerging Opportunities and Challenges for Biologically Inspired Robotic Design [Journal Article]. Micromachines (Basel). 2020;11(4). Available from: https://www.ncbi.nlm.nih.gov/pubmed/32340402. doi:10.3390/mi11040448.

[3] Fountain TWR, Kailat PV, Abbott JJ. Wireless control of magnetic helical microrobots using a rotating-permanent-magnet manipulator. In: 2010 IEEE International Conference on Robotics and Automation; 2010. p. 576-81. doi:10.1109/ROBOT.2010.5509245.

[4] Peyer KE, Tottori S, Qiu F, Zhang L, Nelson BJ. Magnetic helical micromachines [Journal Article]. Chemistry. 2013;19(1):28-38. Available from: https://www.ncbi.nlm.nih.gov/pubmed/23203403. doi:10.1002/chem.201203364.

[5] Garstecki P, Tierno P, Weibel DB, Sagues F, Whitesides GM. Propulsion of flexible polymer structures in a rotating magnetic field [Journal Article]. J Phys Condens Matter. 2009;21(20):204110. Available from:

https://www.ncbi.nlm.nih.gov/pubmed/21825519. doi:10.1088/0953-8984/21/20/204110.

[6] Louisa Hafferl CGSM Leendert-Jan W Ligtenberg, Khalil ISM. Non-Buoyant Microrobots Swimming with Near-Zero Angle of Attack; 2023. .

[7] Ligtenberg LJW, Ekkelkamp I, Halfwerk F, Goulas C, Arens J, Warlé M, et al. Helical Propulsion in Low-Re Numbers with Near-Zero Angle of Attack; 2023. .

[8] Xu L, Gong D, Chen KH, Cai J, Zhang WQ. Acoustic levitation applied for reducing undesired lateral drift of magnetic helical microrobots. Journal of Applied Physics;128(18). doi:Artn 184703 10.1063/5.0026728.

[9] Rodenborn B, Chen CH, Swinney HL, Liu B, Zhang HP. Propulsion of microorganisms by a helical flagellum [Journal Article]. Proc Natl Acad Sci U S A. 2013;110(5):E338-47. Available from: https://www.ncbi.nlm.nih.gov/pubmed/23319607. doi:10.1073/pnas.1219831110.

[10] Gray J, Hancock GJ. The Propulsion of Sea-Urchin Spermatozoa [Journal Article]. Journal of Experimental Biology. 1955;32(4):802-14. doi:https://doi.org/10.1242/jeb.32.4.802.

[11] Mahoney AW, Sarrazin JC, Bamberg E, Abbott JJ. Velocity Control with Gravity Compensation for Magnetic Helical Microswimmers [Journal Article]. Advanced Robotics. 2011;25(8):1007-28. Available from: <Go to ISI>://WOS:000291548500004. doi:10.1163/016918611x568620.

[12] Ye C, Liu J, Wu X, Wang B, Zhang L, Zheng Y, et al. Hydrophobicity Influence on Swimming Performance of Magnetically Driven Miniature Helical Swimmers [Journal Article]. Micromachines (Basel). 2019;10(3). Available from: https://www.ncbi.nlm.nih.gov/pubmed/30845732. doi:10.3390/mi10030175.

[13] Shum H. Microswimmer Propulsion by Two Steadily Rotating Helical Flagella [Journal Article]. Micromachines (Basel). 2019;10(1). Available from: https://www.ncbi.nlm.nih.gov/pubmed/30669288. doi:10.3390/mi10010065.

[14] Brennen C, Winet H. Fluid-Mechanics of Propulsion by Cilia and Flagella [Journal Article]. Annual Review of Fluid Mechanics. 1977;9:339-98. Available from: <Go to ISI>://WOS:A1977CS66100014. doi:DOI 10.1146/annurev.fl.09.010177.002011.

[15] Ligtenberg LJW, Khalil ISM. Input-Output Boundedness of a Magnetically-Actuated Helical Device [Conference Paper]. 2023:5433-8. doi:10.1109/icra48891.2023.10160556.